

Avalanche-size distribution at the depinning transition: A numerical test of the theory

Alberto Rosso,^{1,2} Pierre Le Doussal,² and Kay Jörg Wiese²

¹LPTMS; CNRS and Université Paris-Sud, UMR 8626, 91405 Orsay Cedex, France.

²CNRS-Laboratoire de Physique Théorique de l'École Normale Supérieure, 24 rue Lhomond, 75231 Paris Cedex, France.

(Dated: April 7, 2009)

We calculate numerically the sizes S of jumps (avalanches) between successively pinned configurations of an elastic line ($d = 1$) or interface ($d = 2$), pulled by a spring of (small) strength m^2 in a random-field landscape. We obtain strong evidence that the size distribution, away from the small-scale cutoff, takes the form $P(S) = \frac{\langle S \rangle}{S_m^2} p(S/S_m)$ where $S_m := \frac{\langle S^2 \rangle}{2\langle S \rangle} \sim m^{-d-\zeta}$ is the scale of avalanches, and ζ the roughness exponent at the depinning transition. Measurement of the scaling function $f(s) := s^\tau p(s)$ is compared with the predictions from a recent Functional RG (FRG) calculation, both at mean-field and one-loop level. The avalanche-size exponent τ is found in good agreement with the conjecture $\tau = 2 - 2/(d + \zeta)$, recently confirmed to one loop via the FRG. The function $f(s)$ exhibits a shoulder and a stretched exponential decay at large s , $\ln f(s) \sim -s^\delta$, with $\delta \approx 7/6$ in $d = 1$. The function $f(s)$, universal ratios of moments, and the generating function $\langle e^{\lambda s} \rangle$ are found in excellent agreement with the one-loop FRG predictions. The distribution of *local* avalanche sizes S_ϕ , i.e. of the jumps of a subspace of the manifold of dimension d_ϕ , is also computed and compared to our FRG predictions, and to the conjecture $\tau_\phi = 2 - 2/(d_\phi + \zeta)$.

I. INTRODUCTION

Elastic objects pinned by a random substrate are ubiquitous in nature. The competition between elastic restoring forces and quenched disorder results in multiple metastable states. Upon applying an external force one observes collective jerky motion which proceeds by sudden jumps, called avalanches. Examples are the Barkhausen noise in magnets [1–7], jumps in the creep motion of magnetic domain walls [8–11], avalanches in the depinning of a contact-line of a fluid [12–15], or in dislocation and crack propagation [16–19], and stick-slip motion of e.g. tectonic plates, responsible for earthquakes [20–23]. Avalanches have also been studied in models without quenched substrate disorder, such as in sand-pile models and in granular matter [24–27]. An important characteristic of avalanche motion is its scale invariance, self-organized criticality, and a broad distribution $P(S) \sim S^{-\tau}$ of the sizes S of avalanches, for sizes S between a small- and large-scale cutoff $S_{\min} \ll S \ll S_m$. Pinned elastic manifolds are an important prototype of a much wider class of phenomena, reaching far outside physics, e.g. into economy and finance, where extreme (and sometimes catastrophic) events are sufficiently frequent and large to dominate most observables. In this context, it is clearly of importance to understand how the avalanche-size probability is cut off at the large scales, for $S > S_m$.

Although avalanche motion of pinned manifolds has been studied for a while in numerics [28–30], most work focused on measuring the avalanche-size exponent τ , with minimal guidance from the theory. This is mainly because no analytic approach was available besides mean-field and scaling arguments. The most notable one was proposed by Narayan and Fisher (NF) [31] on the basis of the unproved assumption that the avalanche density

remains finite at the depinning threshold, resulting into

$$\tau = 2 - \frac{2}{d + \zeta}. \quad (1)$$

Here ζ is the roughness exponent at the depinning transition. Progress both in constructing the field theory of the depinning transition [32–35] following the pioneering work on the Functional RG (FRG) [31, 36, 37] and in developing new powerful algorithms [15, 38–43] had focused mostly on structural properties of the pinned manifold, such as the precise determination of ζ . Even an appropriate definition of static and dynamic avalanches, allowing contact with the field theory, had remained unclear. It was given in the statics [44–46] and at depinning [47, 48] using a confining quadratic potential; it led to the measurement, with great accuracy, of the renormalized disorder correlator $\Delta(u)$, i.e. the fixed point of the FRG. Only very recently we succeeded in computing the distribution of avalanche sizes within the FRG [49–51]. The calculation at tree level gave mean-field predictions (some of them new and non-trivial), valid above the upper critical dimension $d_{uc} = 4$, i.e. for $d > 4$. The one-loop calculation gave an expansion to order $O(\epsilon)$, with $\epsilon = 4 - d$. Remarkably, the conjecture (1) was confirmed to $O(\epsilon)$ accuracy. It is thus of great interest to test these predictions in numerics.

The aim of the present paper is to compute numerically the jumps (avalanches) between successively pinned configurations of an elastic line ($d = 1$) and interface ($d = 2$). The convenient setting to compare with the recent predictions from the FRG is to submit the manifold to an external quadratic well, i.e. a spring. We will study mostly random-field disorder, but we also check that the results are the same for random-bond disorder, as is predicted at depinning and was checked in our previous work [48] for the renormalized disorder correlator $\Delta(u)$. Most of the

numerical method is similar to our previous work [48].

The outline of this article is as follows: We define in section II the model and numerical procedure; and in section III an avalanche, its size, the characteristic scales and the scaling functions. In section IV the reader will find our numerical results for the avalanche-size distribution, and their comparison to our analytical results in $d = 1$ and $d = 2$. In section V we compare our numerical and analytical results for the universal ratios of algebraic moments, the r_n . In section VI we do the same for the generating function of exponential moments, i.e. the characteristic function of the size distribution, denoted $\tilde{Z}(\lambda)$, in $d = 1$ and $d = 2$. Finally, in Section (VII), we compute the distribution of local avalanches in $d = 1$ and compare with the predictions.

II. NUMERICAL PROCEDURE: PARABOLA AND METASTABLE STATES

Let us now describe the model and algorithm, in $d = 1$ for simplicity. The procedure is very similar to our previous work [48]. The interface is discretized as $u(x) \equiv u_i$, $i = 1, \dots, L$, and periodic boundary conditions are taken: $u_0 = u_L$, $u_{L+1} = u_1$. We start from a flat interface ($u_i = 0$) embedded in a parabolic potential. The equation of motion is

$$\partial_t u_i = m^2(w - u_i) + u_{i+1} + u_{i-1} - 2u_i + F(i, u_i) \quad (2)$$

$F(i, u_i)$ is the disorder force. We distinguish two different microscopic disorders:

(i) *random force (RF)*: for each integer value of u_i we take a random number extracted from a normal distribution. The value of the random force for non-integer values of u_i is given by the linear interpolation of the forces at the two closest integers u_i . Forces for different i are independent.

(ii) *random bond (RB)*: the random force is derived from a random potential: $F(i, u_i) = -\partial_{u_i} V(i, u_i)$. For each integer value of u_i , the potential is a random number normally distributed. The interpolation of V is done by means of a cubic spline connecting M random numbers. Two extra conditions are needed in order to define a spline: we have taken $F(i, 0) = 0$ and $F(i, M) = 0$. In our simulations $M = 100$. When the line advances beyond $u_i = M$, a new spline, with M new random numbers is generated. Potentials for different i are independent.

The value w is the center of mass of a confining potential for each point i , of the form $\frac{m^2}{2}(w - u_i)^2$. In the simulation, w is increased from 0. For each value of w a metastable state is computed. Increasing w , a stationary sequence of metastable states (independent of the initial configuration) is reached, as observed in Ref. [48]. This is the steady state on which we focus. Our main results concern an elastic string in $d = 1$ of size L with RF disorder, but we have also studied RB disorder, see Fig. 1, and a 2-dimensional elastic interface of size L^2 with periodic boundary conditions. As expected, for the depinning

transition, the RB case falls in the same universality class as the RF case and results are very similar.

III. DEFINITIONS AND OBSERVABLES

For given $w = w_0$ the manifold moves to a metastable state $u_{w_0}(x)$, i.e. a state dynamically stable to infinitesimally small deformations. Following the notation of [49, 50], we define the center of mass of the metastable configuration

$$u(w_0) := \frac{1}{L^d} \int dx u_{w_0}(x) \quad (3)$$

with L the linear size of the system (number of points), and d the dimension. One then increases w , and a smooth forward deformation of $u_w(x)$ results (for smooth short-scale disorder) while the state remains stable. At some $w = w_1$ the state becomes unstable and the manifold, for $w = w_1^+$ moves until it is blocked again in a new metastable state $u_{w_1}(x)$ (also locally stable). This process is called an avalanche and its size S is defined as the area swept by the line as it jumps between the two consecutive metastable states:

$$S := L^d [u(w_1) - u(w_0)] \quad (4)$$

The distribution of avalanche sizes is expected to exhibit universality, i.e. independence of short scales, for sizes $S > S_{\min}$. The short-scale cutoff S_{\min} corresponds to the area spanned by a single monomer on the scale of the discretization of the disorder (in our units $S_{\min} \simeq 1$). In the limit $m = 0$ a critical point is reached, resulting in a power-law distribution of avalanche sizes. To properly define the problem, including the stationary measure, it is essential to consider a small $m > 0$. Then, the internal correlation length L_m is finite: it can e.g. be measured from the structure factor leading to [48]

$$L_m \approx 5/m. \quad (5)$$

L_m is large in the small- m regime considered here. As a result, the distribution of avalanche sizes is cut off by the large scale $S_m \gg S_{\min}$, defined as

$$S_m := \frac{\langle S^2 \rangle}{2\langle S \rangle}. \quad (6)$$

It is expected to scale as $S_m \sim L_m^{d+\zeta} \sim m^{-d-\zeta}$ at small m . Here and below we define the (normalized) distribution of avalanche sizes $P(S)$, as well as its moments

$$\langle S^n \rangle := \frac{1}{N} \sum_{i=1}^N S_i^n = \int_0^\infty dS S^n P(S) \quad (7)$$

from the sequence of measured avalanches S_i , $i = 1, \dots, N$.

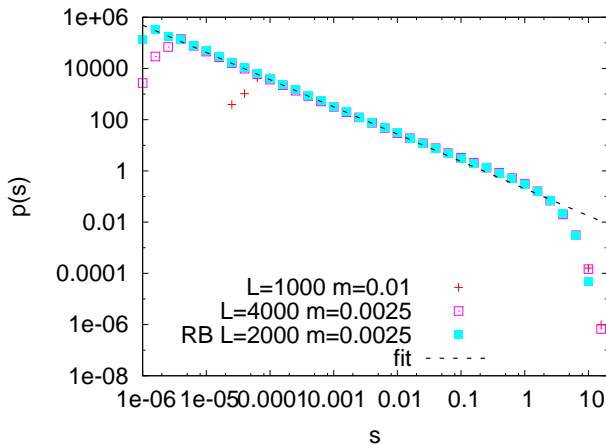


FIG. 1: Random Field and Random Bond (RB) ($d = 1$). A fit with a power law gives the exponent $\tau = 1.08 \pm 0.02$. The agreement with Eq. (12) is discussed in the text.

The scale S_m is important as it allows to define universal functions. In the variable $s := S/S_m$ the avalanche-size distribution should become universal. Indeed, one of the predictions of the FRG theory is that if the exponent τ satisfies $2 > \tau > 1$ which is the case here, then the distribution of avalanche sizes for $S \gg S_{\min}$ takes the form as $m \rightarrow 0$, i.e. $S_m \gg S_{\min}$,

$$P(S)dS := \frac{\langle S \rangle}{S_m} p\left(\frac{S}{S_m}\right) \frac{dS}{S_m}. \quad (8)$$

The function $p(s)$ is universal and depends only on the space dimension d . Note that the normalized probability $P(S)$ depends on the cut-off S_{\min} via the first moment $\langle S \rangle$ which cannot be predicted by the theory, hence is an input from the numerics. It is important to stress that while the function $p(s)$ is universal and convenient for data analysis, *it is not a probability distribution* and is not normalized to unity. Rather, it satisfies from its definition (8) and using (6) the two normalization conditions

$$\langle s \rangle_p = \int ds s p(s) = 1 \quad (9)$$

$$\langle s^2 \rangle_p = \int ds s^2 p(s) = 2. \quad (10)$$

Here and below we use the notation $\langle s \rangle_p$ to denote an integration over $p(s)$ and distinguish it from a true expectation value over $P(S)$, denoted $\langle \dots \rangle$.

IV. THE AVALANCHE-SIZE DISTRIBUTION

The rescaled avalanche-size distribution can be written as

$$p(s) = s^{-\tau} f(s) \quad (11)$$

where τ is the avalanche-size exponent, and $f(s)$ the universal cutoff function [57], which tends to a constant for $s \rightarrow 0$. For the present model, the only analytical prediction prior to our work [49, 50] concerns the exponent τ , via the above mentioned NF [31, 52] conjecture

$$\tau = \tau_{\text{conj}} = 2 - \frac{2}{d + \zeta}, \quad (12)$$

where ζ is the roughness exponent at the depinning transition. Exact solution [21] of a mean field toy model of avalanches, which turns out to be related to the famous Galton process [53] in genealogy, gives an exponent $\tau_{\text{MF}} = 3/2$. This exponent is also the one expected if we replace $d = d_{\text{uc}} = 4$ in the NF conjecture. This does however not constitute a first-principle calculation starting from the model of the pinned interface. The latter was only possible using the FRG [49, 50]. The summation of all tree diagrams within the FRG is shown to be asymptotically exact for $d > 4$ and leads to the mean-field prediction [49, 50] for τ and for the full rescaled avalanche-size distribution (see below).

We now discuss our numerical results starting with the avalanche-size exponent τ . Note that the data in Fig. 1 contain both random-field and random-bond disorder and that, as expected from the universality of the depinning fixed point, the results are indistinguishable. Hence in the following we focus on RF disorder. For $d = 1$, a direct power-law fit of our numerical data (see Fig. 1) gives

$$\tau_{\text{num}}^{d=1} = 1.08 \pm 0.02. \quad (13)$$

This value has to be compared with the conjecture of Eq. (12). The roughness exponent is known numerically with a good accuracy from system sizes ($L \sim 10^3$) and $m = 0$, as $\zeta = 1.26 \pm 0.01$ [40]. This value for ζ gives $\tau_{\text{conj}} = 1.115 \pm 0.005$. Hence the estimate (13) is slightly smaller than the value of τ obtained from the conjecture. There are several possible explanations for this.

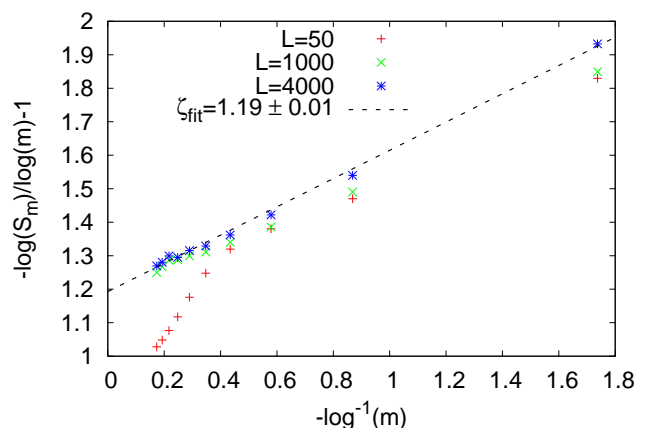


FIG. 2: Numerical extrapolation of the exponent ζ to mass $m = 0$. We find $\zeta = 1.19 \pm 0.01$

First one notes that although (13) is extracted from pieces of $p(s)$ which have already well converged in terms of m and L , the resulting window of sizes is limited. Although we took this into account in estimating (13), we cannot exclude a further small upward shift in the central value as the window size increases.

Second, we have also measured the *effective* ζ exponent for the sizes and masses used here. From measurements of S_m we extract $\zeta = 1.19 \pm 0.01$ as can be seen on Fig. 2. We have checked that comparable estimates can be extracted from the structure factor $S(q)$, as measured also in [48], using fits taking into account the mass. Inserting this value for an effective ζ into Eq. (12), this results in an effective value for $\tau_{\text{conj}} = 1.086 \pm 0.004$, which is in much better agreement with our measured value (13).

Finally, deviations from the conjecture for the *asymptotic* value of τ are still, strictly speaking, possible, but if they exist they must be around or below the error of 0.02 in Eq. (13). This does not rule them out since, as discussed in [50], if present they are expected to be small [58].

Within the FRG [49, 50] it is possible to compute the universal scaling function. For $d > 4$ summation of all tree diagrams gives

$$f_{\text{MF}}(s) = \frac{1}{2\sqrt{\pi}} e^{-s/4}. \quad (14)$$

The one-loop FRG calculation gives

$$f(s) = \frac{A}{2\sqrt{\pi}} \exp\left(C\sqrt{s} - \frac{B}{4}s^\delta\right), \quad (15)$$

with exponents

$$\tau = \frac{3}{2} + \frac{3}{8}\alpha = \frac{3}{2} - \frac{1}{8}(1 - \zeta_1)\epsilon \quad (16)$$

$$\delta = 1 - \frac{\alpha}{4} = 1 + \frac{1}{12}(1 - \zeta_1)\epsilon \quad (17)$$

where $\alpha = -\frac{1}{3}(1 - \zeta_1)\epsilon$ and $\zeta_1 = 1/3$ for the RF class, relevant to the present study. The constants A , B and C depend on ϵ , and must satisfy the normalization conditions (9), (10). At first order in ϵ they are $C = -\frac{1}{2}\sqrt{\pi}\alpha$, $B = 1 - \alpha(1 + \frac{\gamma_E}{4})$, $A = 1 + \frac{1}{8}(2 - 3\gamma_E)\alpha$, $\gamma_E = 0.577216$. As usual, the one-loop results for the exponents τ , δ and for the parameters A , B , and C are exact up to $O(\epsilon^2)$.

To analyze our numerical data for the avalanche-size distribution, we have first computed $\langle S^2 \rangle$ and $\langle S \rangle$ from the data, which allowed to determine numerically the universal (and parameter-free) function $p(s)$ using (6) and (8). Hence by construction the numerical data satisfy conditions (9) and (10). They are plotted in Figs. 3 and 4, with emphasis either on the power-law region or on the tail. Note that for the different values of m and L used here, the data have converged, with the exception of the last point for very large avalanches over-suppressed by the finite size of the interface in the smallest samples, and of the region of very small avalanches, which are cut off at $s \approx 1/S_m$.

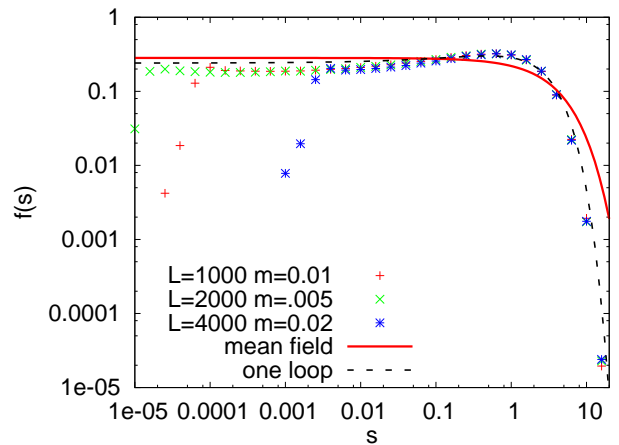


FIG. 3: Random Field ($d = 1$). Blow up of the power-law region. The red solid curve is given by Eq.(14), the black dashed line by Eq.(15), with $A = 0.852$, $B = 1.56$ and $C = 0.56$.

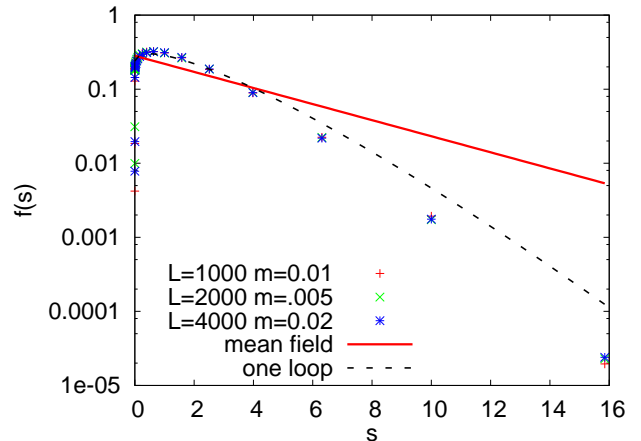


FIG. 4: Random Field ($d = 1$). Blow up of the tail region. The red solid curve is given by Eq.(14), the black dashed line by Eq.(15), with $A = 0.852$, $B = 1.56$ and $C = 0.56$.

To compare the numerical data with the mean-field and one-loop predictions, we use two procedures:

In the first procedure we compare directly the cut-off functions $f(s)$, see Figs. 3 and 4. They are defined as $f(s) := s^\tau p(s)$ where τ is respectively $\tau_{\text{num}} = 1.08$ for the numerical data, $\tau_{\text{MF}} = 3/2$ for the mean-field prediction, and $\tau_{\text{Pade}} = 5/4$ for the simplest Padé approximant of the one-loop result, i.e. setting $\epsilon = 3$ in (16). For $d = 1$, due to the large value of $\epsilon = 3$, the function $p_{1\text{-loop}}(s)$ with $\tau = 5/4$, $\delta = 7/6$, $A = 5/6 - \gamma_E/4$, $B = 5/3 + \gamma_E/6$ and $C = \sqrt{\pi}/3$ does not have the correct normalization. We chose to introduce two rescaling factors

$$p(s) = c_1 p_{1\text{-loop}}(c_2 s) \quad (18)$$

in order to enforce the conditions (9) and (10). This procedure only changes the values of A , B and C in a consistent manner, see Figs. 3 and 4. Note that even though only $f(s)$ is plotted, the chosen value of τ changes

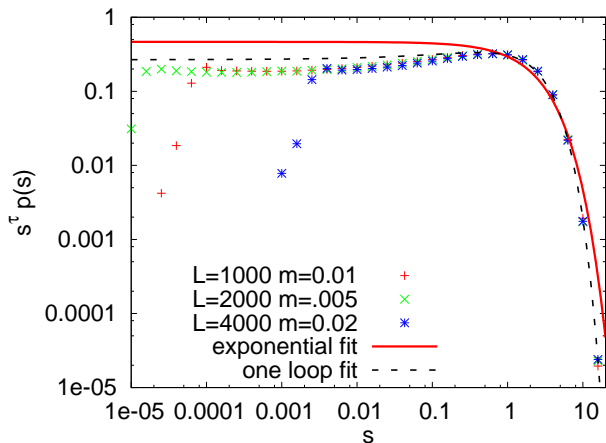


FIG. 5: Random Field ($d = 1$). Blow up of the power-law region. The red solid curve is given by Eq.(19), the black dashed line by Eq.(15), with $A = 0.947$, $B = 1.871$ and $C = 0.606$.

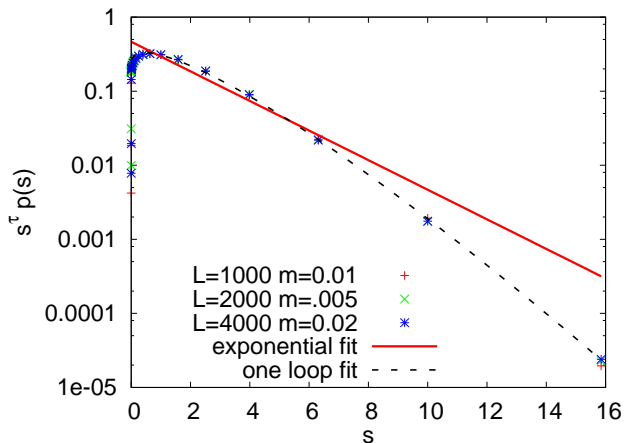


FIG. 6: Random Field ($d = 1$). Blow up of the tail region. The red solid curve is given by Eq.(19), the black dashed line by Eq.(15), with $A = 0.947$, $B = 1.871$ and $C = 0.606$.

the values of A, B, C via the normalization conditions, hence must be discussed accordingly.

A second approach, shown in Figs. 5 and 6, consists in fitting *the same numerical curves* as in Figs. 3 and 4, with either (i) an exponential function (“exponential fit”) or (ii) the one-loop function (“fit one loop”), but using the numerically obtained exponent $\tau = \tau_{\text{num}} = 1.08$. The exponential fit reads

$$p(s)s^\tau = \frac{\left(1 - \frac{\tau}{2}\right)^{2-\tau}}{\Gamma(2-\tau)} \exp\left(\left(-1 + \frac{\tau}{2}\right)s\right). \quad (19)$$

All coefficients are determined as a function of τ by the normalization conditions (9) and (10). Note that this exponential fit is mostly a guide to emphasize the sub-exponential tail apparent in the data. Similarly, for the one-loop fit we adopt the procedure described in the previous paragraph, with $\tau = \tau_{\text{num}}$ everywhere instead of

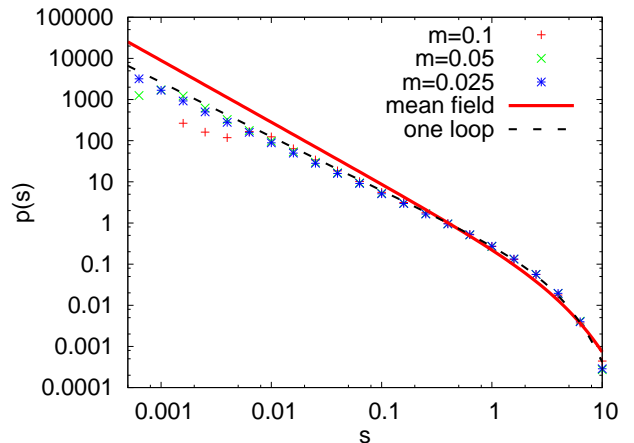


FIG. 7: Random Field ($d = 2$, $L = 100$ for $m = 0.1, 0.05$; $L = 200$ for $m = 0.025$). A fit with a power law gives access to the exponent $\tau = 1.3 \pm 0.01$. The comparison with Eq.(12) is discussed in the text.

the one-loop Padé value $\tau = 5/4$. We expect this fit to be less sensitive to the lack of precision in the one-loop estimate of τ for the large value of $\epsilon = 3$ relevant here, and to better capture the tail region. This is indeed what is found, see Fig. 6. It confirms the sub-exponential tail exponent $\delta \approx 7/6$ to a rather good precision. We stress that our procedure is *not a fit* using A, B, C as fit parameters, but that *all* parameters are specified by the one-loop prediction.

We now turn to a 2-dimensional interface. The universal function $p(s)$ for $d = 2$ and RF disorder is plotted on Fig. 7. From a direct power-law fit, we find

$$\tau_{\text{num}}^{d=2} = 1.3 \pm 0.02. \quad (20)$$

This value has to be compared with the conjecture of Eq. (12). The roughness exponent at the depinning transition is known numerically as $\zeta_{\text{num}}^{d=2} = 0.753 \pm 0.002$ [40], which gives $\tau_{\text{conj}}^{d=2} = 1.2735 \pm 0.0005$. Although our value (20) of τ is compatible with the conjecture, the precision is insufficient to conclude on possible small deviations from the latter. The mean-field and one-loop predictions discussed above are plotted for comparison, using the simplest one-loop Padé approximant, i.e. $\alpha = -4/9$, $\tau = 4/3$, $\delta = 10/9$. After the above described procedure (18) using the normalization conditions (9) and (10) this led to the values $A = 0.92$, $B = 1.416$ and $C = 0.383$.

V. UNIVERSAL MOMENT RATIOS r_n

Important universal quantities characterizing the avalanche statistics are the following universal ratios of

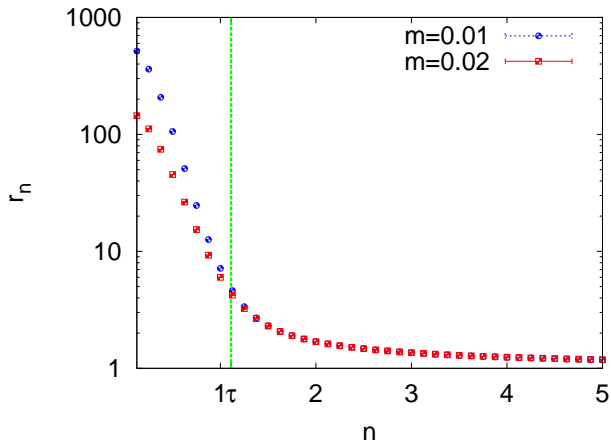


FIG. 8: Numerical values of the ratios r_n for bare random-field disorder ($d = 1$, $L = 2000$), and $m = 0.02$, $m = 0.01$. For $m = 0$ a pole is expected for $n = \tau$. For $n < \tau$ the divergence manifests itself through the data's dependence on m .

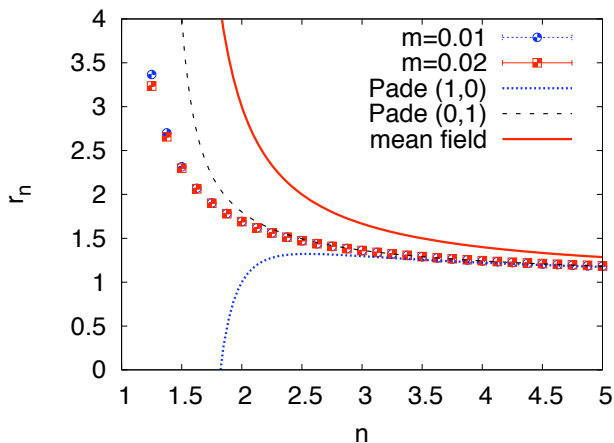


FIG. 9: Random Field ($d = 1$, $L = 2000$). Moment ratios r_n : comparison between numerics and analytic predictions

avalanche-size moments:

$$r_n := \frac{\langle S^{n+1} \rangle \langle S^{n-1} \rangle}{\langle S_n \rangle^2} = \frac{\langle s^{n+1} \rangle_p \langle s^{n-1} \rangle_p}{\langle s_n \rangle_p^2}. \quad (21)$$

Here n can be non-integer. As shown in [50] all non-universal scales disappear in the ratios r_n . Our numerical findings are summarized in Fig. 8. The pole expected at $n = \tau \approx 1.08$ in the limit of infinite S_m/S_{\min} manifests itself in a non-convergence of the numerical data upon lowering m . This is an independent method for calculating τ .

We now compare to the FRG calculation [50]. The function r_n can be evaluated in an $\epsilon = 4 - d$ expansion. At the mean-field level ($\epsilon = 0$)

$$r_n^0 = \frac{2n - 1}{2n - 3}, \quad (22)$$

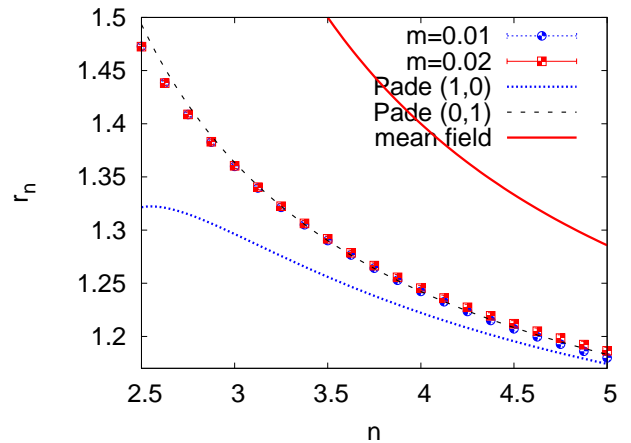


FIG. 10: Random Field ($d = 1$, $L = 2000$). Moment ratios r_n : blow up of the tail behavior. The mean field behavior is given by Eq.(22). The Padé (1,0) by Eq(23) and the Padé (0,1) is also plotted.

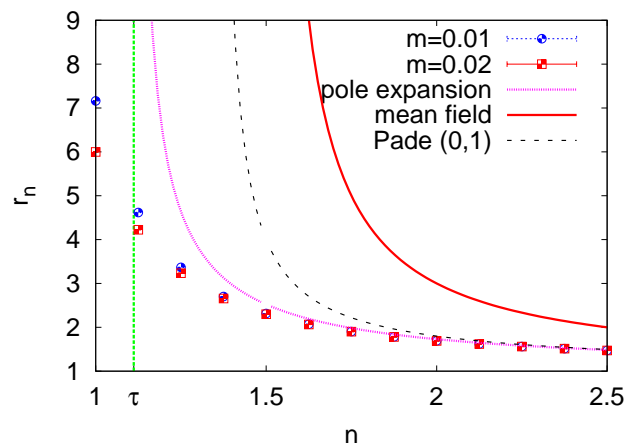


FIG. 11: Random Field ($d = 1$, $L = 2000$). Moment ratios r_n : blow up around the pole and comparison with Eq. (24).

and a pole is found for $n = \tau_{\text{MF}} = 3/2$.

The one-loop ϵ expansion leads to the following expression [50]:

$$r_n^{1\text{-loop}} = r_n^{\text{MF}} - \frac{\epsilon}{3}(1 - \zeta_1) \frac{n\Gamma(n - \frac{3}{2}) + \sqrt{\pi}\Gamma(n - 1)}{(2n - 3)^2\Gamma(n - \frac{3}{2})}, \quad (23)$$

where $\zeta_1 = 1/3$ for RF. This expression corresponds to the Padé (1,0) in the ϵ -expansion; we also use the Padé (0,1). The comparison with the data is shown on Fig. 9. For the large-moment region, a blow-up is shown on Fig. 10. The agreement of the data with the two one-loop Padé approximants, as compared to mean field, is quite striking.

However, both Padés break down close to $n = \tau$. We give another useful form for comparison to numerics. The idea is to isolate the simple pole which occurs in any

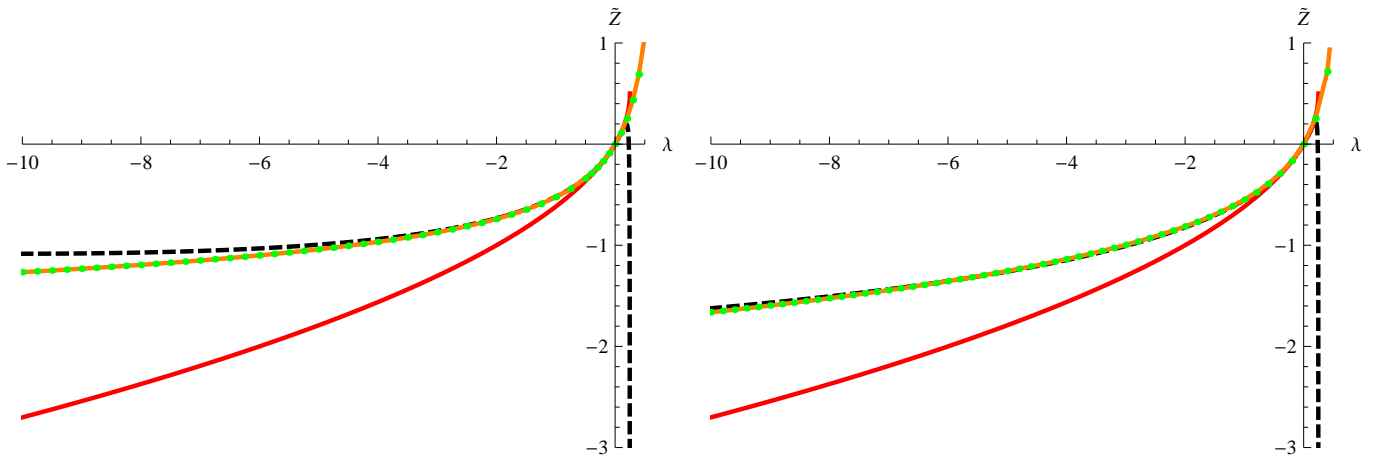


FIG. 12: The characteristic function $\tilde{Z}(\lambda)$ for $d = 1$ (left) and $d = 2$ (right). Mean field (solid red/grey) from Eq. (29); one-loop from Eq. (30) (dashed black); and numerical results for $L = 4000, m = 0.0005$ (solid orange/green dots). The singularity in (29) and (30) for $\lambda = 1/2$ (indicated by a vertical dotted line) is smoothed out in the numerics, see figure 13 for details.

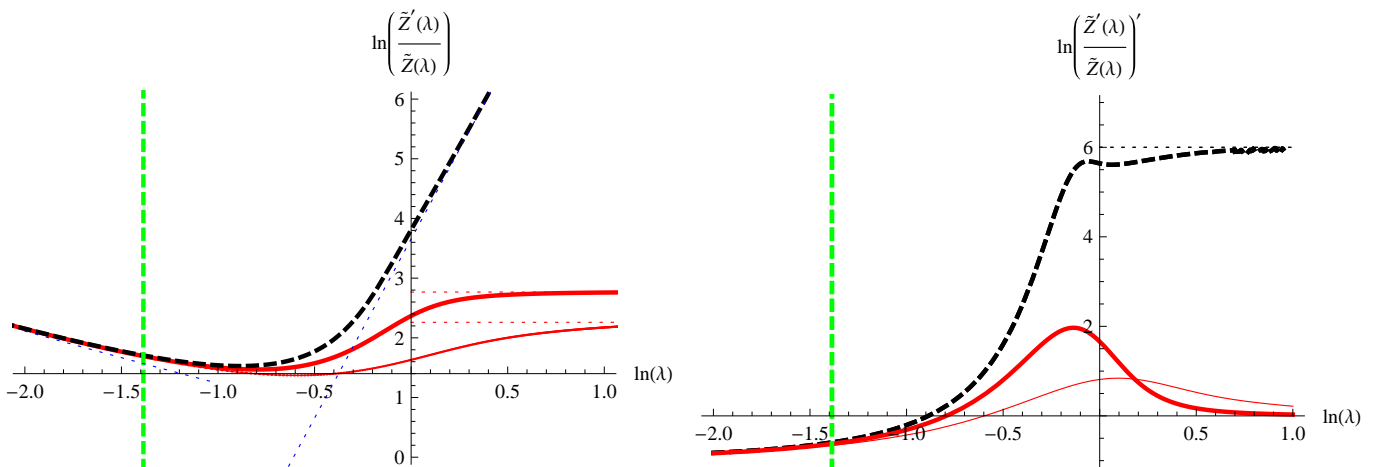


FIG. 13: Left: Log-log plot of $\partial_\lambda \ln \tilde{Z}(\lambda)$ versus λ . For large λ , we expect from Eq. (15) that the analytic result (black, thick, dashed) obtained by integrating Eq. (28) numerically, has slope $1/(\delta - 1)$ (blue dotted line is this asymptotic). The numerical results are for $L = 4000$ and $m = 0.02$ (thick red) and $m = 0.00125$ (thin red). For large λ , $\tilde{Z}_{\text{num}}(\lambda) \approx \frac{S_m}{\langle S \rangle} \frac{1}{N} \exp(\lambda S_{\text{max}})$, where S_{max} is the largest avalanche encountered in the simulation, and the curve saturates (dotted red lines). The larger S_{max}/S_m , the better the data. For $m = 0.02$ (thick red) this ratio is 16, whereas for $m = 0.00125$ (thin red) it is 10. The vertical dashed green line indicates the location $\lambda = 1/4$ of the singularity in $\tilde{Z}(\lambda)$ at the mean-field level. Right: Slope of the function left, i.e. the effective exponent $1/(\delta - 1)$. One sees that the effective exponent increases with increasing S_{max}/S_m . Our data, which clearly have not converged in terms of S_{max}/S_m , allow to estimate $1 < \delta \leq \frac{3}{2}$ from the maximum slope.

dimension, as

$$r_n = \frac{A_d}{n - \tau} + B_{n,d}. \quad (24)$$

Up to $O(\epsilon^2)$ corrections [50]

$$A_d = 1 - \frac{1 + \pi}{12}(1 - \zeta_1)\epsilon \quad (25)$$

$$B_{n,d} = 1 + \frac{\pi\Gamma(n - \frac{1}{2}) - \sqrt{\pi}\Gamma(n - 1)}{6(2n - 3)\Gamma(n - \frac{1}{2})}(1 - \zeta_1)\epsilon. \quad (26)$$

In Fig. 11 this formula is plotted setting $\epsilon = 3$. It shows that it works quite well, even close to the pole at $n = \tau$.

VI. THE CHARACTERISTIC FUNCTION $\tilde{Z}(\lambda)$

It is useful to define a generating function of exponential moments, i.e. the characteristic function of the avalanche-size probability. Using the definitions (6) and (7), we define the normalized generating function $\tilde{Z}(\lambda)$

$$\tilde{Z}(\lambda) := \frac{S_m}{\langle S \rangle} \frac{1}{N} \sum_{i=1}^N \left[e^{\lambda S_i / S_m} - 1 \right] \quad (27)$$

By construction, $\tilde{Z}(\lambda) = \lambda + \lambda^2 + \dots$. Since large negative λ probe small avalanches, it is expected to be universal for $\lambda \gg -1/S_{\text{min}}$. In the universal range, its relation to

$p(s)$ is

$$\tilde{Z}(\lambda) = \int_0^\infty ds p(s) (e^{\lambda s} - 1) . \quad (28)$$

It has been calculated in [49, 50] at the mean-field level:

$$\tilde{Z}_{1\text{-loop}}(\lambda) = \frac{1}{2} \left(1 - \sqrt{1 - 4\lambda}\right) + \frac{\left((3\lambda + \sqrt{1 - 4\lambda} - 1) \log(1 - 4\lambda) - 2(2\lambda + \sqrt{1 - 4\lambda} - 1)\right) \alpha}{4\sqrt{1 - 4\lambda}} + O(\alpha^2) . \quad (30)$$

where, as above, $\alpha = -\frac{1-\zeta_1}{3}\epsilon = -\frac{2}{9}\epsilon$. The comparison between theory and numerical data is presented on Fig. 12, both for $d = 1$, and $d = 2$. In these figures we have plotted (30), discarding the term $O(\alpha^2)$ and setting $\epsilon = 3$ and $\epsilon = 2$ respectively. The plots show that the simplest extrapolation of the 1-loop correction is extremely good in calculating the behavior even for large negative λ , as was already observed in the static case in [49]. It would be interesting to compare $\tilde{Z}(\lambda)$ for both cases numerically.

For large λ , $\tilde{Z}(\lambda)$ is dominated by the largest avalanche S_{\max} . If $S_{\max}/S_m \gg 1$, then the tail-exponent δ can in principle be extracted from the derivative of $\ln \tilde{Z}(\lambda)$, i.e. $\partial_\lambda \ln \tilde{Z}(\lambda) \sim \lambda^{1/(\delta-1)}$ in some window of λ before it eventually saturates to a constant $\sim S_{\max}$ at larger λ . Our data, which are plotted on Fig. 12, are not yet converged in terms of the ratio S_{\max}/S_m , but are sufficient to give the bound $1 < \delta \leq \frac{3}{2}$. One finally notes that although mean field works better for $d = 2$ than for $d = 1$, the 1-loop corrections are necessary to account for the numerical data.

VII. LOCAL AVALANCHE-SIZE DISTRIBUTION

In [50], we have considered the following definition of the size of a local avalanche S_ϕ :

$$S_\phi = \int d^d x \phi(x) [u_{w_1}(x) - u_{w_0}(x)] . \quad (31)$$

Here we also define:

$$S_m^\phi := \frac{\langle S_\phi^2 \rangle}{2 \langle S_\phi \rangle} \quad (32)$$

Of particular interest is the cross-section with a co-dimension one hyper-plane i.e. $\phi(x) = m^{-1}\delta(x_1)$, or more generally, with a co-dimension d' subspace. This cross-section has dimension $d_\phi = d - d'$. We have chosen the factor of m in the definition of ϕ such that S_m and S_m^ϕ both scale as $m^{-d-\zeta}$. For $d = 1$ we consider a point, i.e. $d' = 1$, $d_\phi = 0$. Note that we always chose the factor of

$$\tilde{Z}_{\text{MF}}(\lambda) = \frac{1}{2} \left(1 - \sqrt{1 - 4\lambda}\right) . \quad (29)$$

At 1-loop order, it reads [49, 50]

m in the definition of ϕ (see above) such that S_m and S_m^ϕ both scale as $m^{-d-\zeta}$.

For a more convenient comparison with numerics, we adopt a slightly different normalization as in Ref. [50], and chose to normalize using S_m^ϕ rather than S_m . We estimate below the ratio $a_\phi = S_m^\phi/S_m$ which allows to go from one set of definitions to the other. Hence the (normalized) local avalanche-size distribution $P^\phi(S^\phi)$ is expected to take the form

$$P^\phi(S^\phi) = \frac{\langle S^\phi \rangle}{(S_m^\phi)^2} p_\phi \left(\frac{S^\phi}{S_m^\phi} \right) . \quad (33)$$

where the universal function $p_\phi(x) = a_\phi^2 \frac{S_m}{\langle S_\phi \rangle} p^\phi(a_\phi x)$ in terms of the one defined in [50] and called p^ϕ there. By construction $p_\phi(x)$ satisfies the normalizations (9) and (10). Similarly we define the generating function as

$$\hat{Z}(\lambda) := \frac{S_m^\phi}{\langle S^\phi \rangle} \frac{1}{N} \sum_{i=1}^N \left[e^{\lambda S_i^\phi / S_m^\phi} - 1 \right] , \quad (34)$$

which reads $\hat{Z}(\lambda) = a_\phi \tilde{Z}^\phi(\lambda/a_\phi)$ in terms of the one defined in [50].

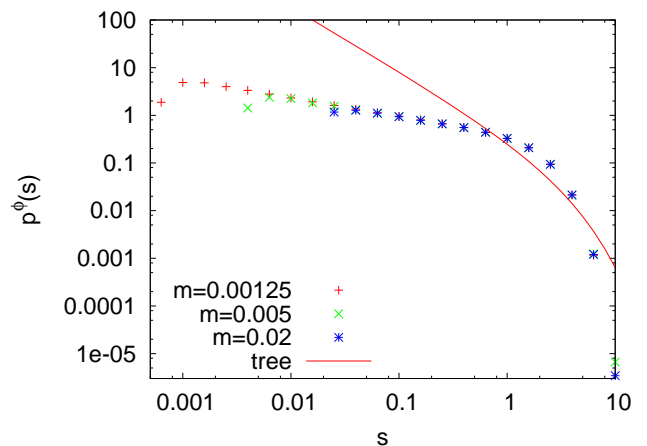


FIG. 14: Random Field ($d = 1$, $d_\phi = 0$, $L = 4000$). From the fit we get $\tau_\phi = 0.39 \pm 0.01$.

At present time we have only three analytical results available to compare the numerical data on local avalanche-size distributions. First the conjecture put forward in [50] and which generalizes (12) reads:

$$\tau_\phi = 2 - \frac{2}{d_\phi + \zeta} \quad (35)$$

where we recall that $d_\phi = d - d'$. Our numerical data for the point on a $d = 1$ string (i.e. one monomer) is shown on Fig. 14 and we find $\tau_\phi = 0.39 \pm 0.01$. If we use the best present estimate $\zeta = 1.26 \pm 0.01$ we find $\tau_\phi^{\text{conj}} = 0.413 \pm 0.01$. If we use the value of $\zeta = 1.19 \pm 0.01$ extracted from the scaling of S_m , we find $\tau_\phi^{\text{conj}} = 0.32 \pm 0.02$. While the values are roughly consistent, the precision on ζ is crucial for a precise comparison. Inverting the conjecture (35), the measurement of $\tau_\phi = 0.39 \pm 0.01$ leads to a conjectured $\zeta = 1.24 \pm 0.01$. For a detailed discussion of the possible artifacts we refer to the discussion in Section IV.

The second result is the exact expression of $\hat{Z}(\lambda)$ and $p_\phi(s)$ in mean field, i.e. for $d \geq 4$ and $d' = 1$. This involves a non-trivial summation of momentum-dependent tree diagrams using instanton calculus. It yields [50] that $\hat{Z}(\lambda)$ is given by the solution of

$$(\hat{Z} - 3)\hat{Z}(2\hat{Z} - 3) = 9\lambda, \quad (36)$$

which vanishes at $\lambda = 0$. This yields the series expansion $\hat{Z}(\lambda) = \lambda + \lambda^2 + \frac{16}{9}\lambda^3 + \frac{35}{9}\lambda^4 + \frac{256}{27}\lambda^5 + O(\lambda^6)$. We have compared this mean-field prediction and the numerical results in $d = 1$, $d_\phi = 0$ on figure 15. It is clear that loop corrections, yet to be computed, will play an important role, as was the case for bulk avalanches, see Fig. 12. The function $p_\phi(s)$, as defined here, is found to be [50] in mean field (i.e. at tree level)

$$p_\phi^{\text{MF}}(s) = \frac{K \frac{1}{3} \left(\frac{s}{2\sqrt{3}} \right)}{2\pi s}. \quad (37)$$

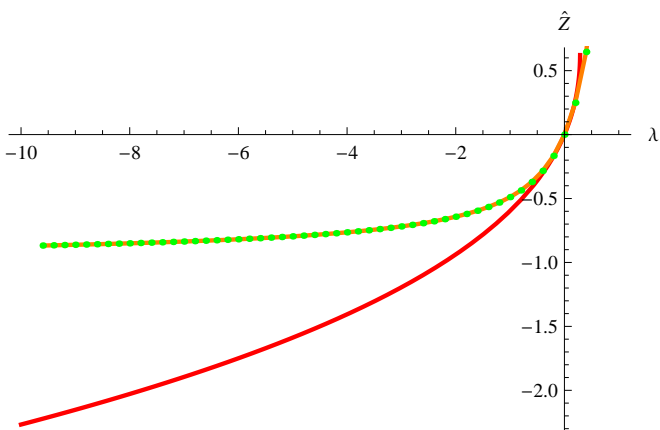


FIG. 15: $\hat{Z}(\lambda)$ both at the tree-level (solid/red), and numerically (green/orange dots), for RF disorder, $m = 0.00125$, $d = 1$, $d_\phi = 0$.

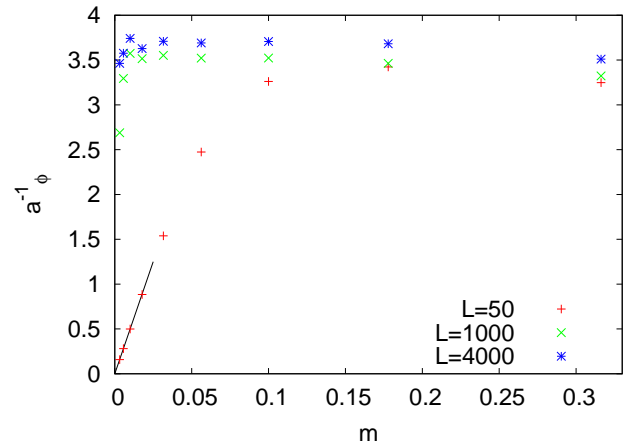


FIG. 16: $1/a_\phi$ as defined in equation (38) and discussed below. For $m \ll 5/L$, $1/a_\phi \approx Lm$.

It satisfies the normalizations (9) and (10), and is related to $\hat{Z}(\lambda)$ via $\hat{Z}(\lambda) = \int_0^\infty ds p_\phi(s) (e^{\lambda s} - 1)$.

Finally, the mean-field calculation [50] also gives:

$$a_\phi := \frac{S_m^\phi}{S_m} = \frac{1}{4} \quad (38)$$

Corrections at 1-loop order slightly decrease this ratio. The ϵ expansion predicts [54]

$$a_\phi = \frac{1}{4} + \alpha \left(1 + \frac{7\pi}{6\sqrt{3}} - \pi \right) + O(\epsilon^2) \quad (39)$$

with $\alpha = -\frac{\epsilon}{3}(1 - \zeta_1)$ and $\alpha = -2/3$ here. Using the two Padé approximants gives the estimate $1/a_\phi = 3.74 \pm 0.01$ which is consistent with the numerically observed value of $1/a_\phi^{\text{num}} = 3.7 \pm 0.05$ for $L = 4000$, $m = 0.00125$.

VIII. CONCLUSION

In this article, we have compared the numerically obtained avalanche-size statistics at the depinning transition with the recent predictions from the functional RG based on an $\epsilon = 4 - d$ expansion. The critical point of the depinning transition for an interface of internal dimensions $d = 1$ and $d = 2$, driven quasi-statically in a random landscape in presence of an external quadratic well of curvature m^2 , is reached in the limit of $m \rightarrow 0$. We have shown that the avalanche-size distribution $P(S)$ takes the expected scaling form with the upper cutoff scale $S_m \sim m^{-d-2\zeta}$, involving a universal function $p(s)$ in the rescaled variable $s = S/S_m$. As we confirmed, it does not depend on whether the microscopic disorder is of random-field or random-bond type. We have computed numerically the function $p(s)$, its moments and its characteristic function and found in all cases good to excellent agreement with the predictions of the 1-loop FRG based on the extrapolation to $d = 1$ and $d = 2$. We have also

studied, for $d = 1$, the *local* avalanches, and there too, we found a rather satisfactory agreement with available analytical predictions. However, it remains an outstanding challenge to compute the local avalanche-size distribution within the FRG beyond mean-field.

Some fine points deserve discussion and further study. First we have not found any clear-cut signature that the conjecture for the avalanche exponent τ be violated at depinning. However, we can not rule out such a violation below a 0.02 precision in τ . A better numerical determination of τ , comparable in precision to the one which exists for the roughness ζ at $m = 0$ would be crucial to confirm or invalidate the conjectured relation between τ and ζ . Presently, the mass, i.e. the quadratic well, appears necessary for a proper definition of the steady state, but unfortunately, this hampers the attempts at a more precise determination of τ .

Second, there has been a recent proposal, in the case of the random-field Ising model [55], that avalanche-size distributions for statics and depinning are described by the same universal functions. Although the physics underlying this hypothesis is not clear to us, one may still ask the question for the present model [59]. One may for instance compare our present results to the one in the statics in [49]. Currently, our precision is not sufficient to conclude. For instance, in $d = 2$ and for RF disorder, the conjecture (1) for τ gives $\tau = 1.25$ for the

statics and $\tau = 1.2735 \pm 0.0005$ for depinning, which are difficult to distinguish numerically. We simply note that both statics and depinning data are in good agreement with extrapolations from the 1-loop FRG [50, 51], but it remains to be analyzed at two loops. As noted previously, since the roughness exponents are different, if the conjecture holds both in the statics and driven dynamics, then the avalanche-size exponents, and presumably the associated distributions, cannot be the same. We leave these subtle questions for the future.

To conclude, it is highly satisfactory that the functional-RG field theory for the avalanche statistics passes all numerical tests. Other interesting observables can now be computed numerically, and studied on a more solid footing, such as the distribution of lateral sizes, or correlations between avalanches. These provide a motivation to further develop the theory. Finally we hope that our present work will motivate similar studies in experiments.

Acknowledgments

This work was supported by ANR under program 05-BLAN-0099-01.

-
- [1] J. S. Urbach, R. C. Madison and J. T. Markert, *Interface depinning, self-organized criticality, and the barkhausen effect*, Phys. Rev. Lett. **75** (1995) 276–279.
 - [2] AP. Mehta, AC. Mills, KA. Dahmen and JP. Sethna, *Universal pulse shape scaling function and exponents: Critical test for avalanche models applied to Barkhausen noise*, Phys. Rev. E **65** (2002) 046139.
 - [3] KA. Dahmen, JP. Sethna, MC. Kuntz and O. Perkovic, *Hysteresis and avalanches: phase transitions and critical phenomena in driven disordered systems*, Journal Of Magnetism And Magnetic Materials **226** (2001) 1287–1292.
 - [4] JH. Carpenter, KA. Dahmen, JP. Sethna, G. Friedman, S. Loverde and A. Vanderveld, *Subloops, Barkhausen noise, and disorder induced critical behavior*, Journal Of Applied Physics **89** (2001) 6799–6801.
 - [5] KA. Dahmen, JP. Sethna and O. Perkovic, *Hysteresis, Barkhausen noise, and disorder induced critical behavior*, Ieee Transactions On Magnetism **36** (2000) 3150–3154.
 - [6] O. Perkovic, K. Dahmen and JP. Sethna, *Avalanches, barkhausen noise, and plain old criticality*, Phys. Rev. Lett. **75** (1995) 4528–4531.
 - [7] K. Dahmen, S. Kartha, JA. Krumhansl, BW. Roberts, JP. Sethna and JD. Shore, *Disorder-driven 1st-order phase-transformations - a model for hysteresis*, Journal Of Applied Physics **75** (1994) 5946–5948.
 - [8] S. Lemerle, J. Ferré, C. Chappert, V. Mathet, T. Giamarchi and P. Le Doussal, *Domain wall creep in an Ising ultrathin magnetic film*, Phys. Rev. Lett. **80** (1998) 849.
 - [9] V. Repain, M. Bauer, J.-P. Jamet, J. Ferré, A. Mougin, C. Chappert and H. Bernas, *Creep motion of a magnetic wall: Avalanche size divergence*, EPL (Europhysics Letters) **68** (2004) 460–466.
 - [10] P. J. Metaxas, J. P. Jamet, A. Mougin, M. Cormier, J. Ferre, V. Baltz, B. Rodmacq, B. Dieny and R. L. Stamps, *Creep and flow regimes of magnetic domain-wall motion in ultrathin pt/co/pt films with perpendicular anisotropy*, Phys. Rev. Lett. **99** (2007) 217208.
 - [11] JP. Sethna, KA. Dahmen and CR. Myers, *Crackling noise*, Nature **410** (2001) 242–250.
 - [12] A. Prevost, E. Rolley and C. Guthmann, *Dynamics of a helium-4 meniscus on a strongly disordered cesium substrate*, Phys. Rev. B **65** (2002) 064517/1–8.
 - [13] A. Prevost, E. Rolley and C. Guthmann, *Thermally activated motion of the contact line of a liquid ⁴He meniscus on a cesium substrate*, Phys. Rev. Lett. **83** (1999) 348–51.
 - [14] S. Moulinet, C. Guthmann and E. Rolley, *Roughness and dynamics of a contact line of a viscous fluid on a disordered substrate*, Eur. Phys. J. A **8** (2002) 437–43.
 - [15] S. Moulinet, A. Rosso, W. Krauth and E. Rolley, *Width distribution of contact lines on a disordered substrate*, Phys. Rev. E **69** (2004) 035103, cond-mat/**0310173**.
 - [16] P. Moretti, M.C. Miguel, M. Zaiser and S. Zapperi, *Depinning transition of dislocation assemblies: Pileups and low-angle grain boundaries*, Phys. Rev. B **69** (2004) 214103.
 - [17] L. Ponsion, D. Bonamy and E. Bouchaud, *Two-dimensional scaling properties of experimental fracture surfaces*, Phys. Rev. Lett. **96** (2006).

- [18] L. Ponson, *Crack propagation in disordered materials: How to decipher fracture surfaces*, Ann. Phys. **32** (2007) 1–128.
- [19] D. Bonamy, S. Santucci and L. Ponson, *Crackling dynamics in material failure as the signature of a self-organized dynamic phase transition*, Phys. Rev. Lett. **101** (2008) 045501.
- [20] D.S. Fisher, K. Dahmen, S. Ramanathan and Y. Ben-Zion, *Statistics of earthquakes in simple models of heterogeneous faults*, Phys. Rev. Lett. **78** (1997) 4885–4888.
- [21] D.S. Fisher, *Collective transport in random media: from superconductors to earthquakes*, Phys. Rep. **301** (1998) 113–150.
- [22] JM. Schwarz and DS. Fisher, *Depinning with dynamic stress overshoots: A hybrid of critical and pseudohysteretic behavior*, Phys. Rev. E **67** (2003) 021603.
- [23] E. A. Jagla and A. B. Kolton, *The mechanisms of spatial and temporal earthquake clustering*, arXiv:**0901.1907** (2009).
- [24] C. Tang and P. Bak, *Mean field-theory of self-organized critical phenomena*, Journal Of Statistical Physics **51** (1988) 797–802.
- [25] Deepak Dhar and Ramakrishna Ramaswamy, *Exactly solved model of self-organized critical phenomena*, Phys. Rev. Lett. **63** (1989) 1659–1662.
- [26] S. Banerjee, S. B. Santra and I. Bose, *Size distribution of different types of sites in abelian sandpile avalanches*, Z. Phys. B **96** (1995) 571–575.
- [27] D. Dhar, *Theoretical studies of self-organized criticality*, Physica A **369** (2006) 29–70.
- [28] O. Narayan and A.A. Middleton, *Avalanches and the renormalization-group for pinned charge-density waves*, Phys. Rev. B **49** (1994) 244–256.
- [29] F. Lacombe, S. Zapperi and H.J. Herrmann, *Force fluctuation in a driven elastic chain*, Phys. Rev. B **63** (2001) 104104 (7 pages).
- [30] A. Tanguy, M. Gounelle and S. Roux, *From individual to collective pinning: Effect of long-range elastic interactions*, Phys. Rev. E **58** (1998) 1577–90.
- [31] O. Narayan and D.S. Fisher, *Threshold critical dynamics of driven interfaces in random media*, Phys. Rev. B **48** (1993) 7030–42.
- [32] P. Chauve, P. Le Doussal and K.J. Wiese, *Renormalization of pinned elastic systems: How does it work beyond one loop?*, Phys. Rev. Lett. **86** (2001) 1785–1788, cond-mat/**0006056**.
- [33] P. Le Doussal, K.J. Wiese and P. Chauve, *2-loop functional renormalization group analysis of the depinning transition*, Phys. Rev. B **66** (2002) 174201, cond-mat/**0205108**.
- [34] P. Le Doussal and K.J. Wiese, *Higher correlations, universal distributions and finite size scaling in the field theory of depinning*, Phys. Rev. E **68** (2003) 046118, cond-mat/**0301465**.
- [35] A. Fedorenko, P. Le Doussal and K.J. Wiese, *Universal distribution of threshold forces at the depinning transition*, Phys. Rev. E **74** (2006) 041110, cond-mat/**0607229**.
- [36] T. Nattermann, S. Stepanow, L.H. Tang and H. Leschhorn, *Dynamics of interface depinning in a disordered medium*, J. Phys. II (France) **2** (1992) 1483–1488.
- [37] H. Leschhorn, T. Nattermann, S. Stepanow and L.H. Tang, *Driven interface depinning in a disordered medium*, Ann. Physik **6** (1997) 1–34.
- [38] A. Rosso and W. Krauth, *Origin of the roughness exponent in elastic strings at the depinning threshold*, Phys. Rev. Lett. **87** (2001) 187002.
- [39] A. Rosso and W. Krauth, *Roughness at the depinning threshold for a long-range elastic string*, Phys. Rev. E **65** (2002) 025101.
- [40] A. Rosso, A.K. Hartmann and W. Krauth, *Depinning of elastic manifolds*, Phys. Rev. E **67** (2003) 021602, cond-mat/**0207288**.
- [41] A. Rosso, W. Krauth, P. Le Doussal, J. Vannimenus and K.J. Wiese, *Universal interface width distributions at the depinning threshold*, Phys. Rev. E **68** (2003) 036128, cond-mat/**0301464**.
- [42] C.J. Bolech and A. Rosso, *Universal statistics of the critical depinning force of elastic systems in random media*, Phys. Rev. Lett. **93** (2004) 125701, cond-mat/**0403023**.
- [43] AB. Kolton, A. Rosso and T. Giamarchi, *Creep motion of an elastic string in a random potential*, Phys. Rev. Lett. **94** (2005) 047002, cond-mat/**0408284**.
- [44] P. Le Doussal, *Finite temperature Functional RG, droplets and decaying Burgers turbulence*, Europhys. Lett. **76** (2006) 457–463, cond-mat/**0605490**.
- [45] A.A. Middleton, P. Le Doussal and K.J. Wiese, *Measuring functional renormalization group fixed-point functions for pinned manifolds*, Phys. Rev. Lett. **98** (2007) 155701, cond-mat/**0606160**.
- [46] P. Le Doussal, *Exact results and open questions in first principle functional RG*, arXiv:**0809.1192** (2008).
- [47] P. Le Doussal and K.J. Wiese, *How to measure Functional RG fixed-point functions for dynamics and at depinning*, EPL **77** (2007) 66001, cond-mat/**0610525**.
- [48] A. Rosso, P. Le Doussal and K.J. Wiese, *Numerical calculation of the functional renormalization group fixed-point functions at the depinning transition*, Phys. Rev. B **75** (2007) 220201, cond-mat/**0610821**.
- [49] P. Le Doussal, A.A. Middleton and K.J. Wiese, *Statistics of static avalanches in a random pinning landscape*, arXiv:**0803.1142** (2008).
- [50] P. Le Doussal and K.J. Wiese, *Size distributions of shocks and static avalanches from the functional renormalization group*, arXiv:**0812.1893** (2008).
- [51] A.A. Fedorenko, P. Le Doussal and K.J. Wiese, in preparation.
- [52] O. Narayan and D.S. Fisher, *Nonlinear fluid flow in random media: critical phenomena near threshold*, Phys. Rev. B **49** (1993) 9469–502.
- [53] H.W. Watson and F. Galton, *On the probability of the extinction of families*, Journal of the Anthropological Institute of Great Britain **4** (1875) 138–144.
- [54] P. Le Doussal and K.J. Wiese, to be published.
- [55] Y. Liu and K.A. Dahmen, *Random field ising model in and out of equilibrium*, cond-mat/**0609609** (2006).
- [56] P. Le Doussal and K.J. Wiese, *Driven particle in a random landscape: disorder correlator, avalanche distribution and extreme value statistics of records*, arXiv:**0808.3217** (2008).
- [57] by universal we mean w.r.t. short scale details. Of course this function is characteristic of a large scale cutoff provided by a parabolic well
- [58] Note that the exact solution in $d = 0$ [56] shows that the conjecture is valid for RF disorder with sufficiently LR correlations (e.g. $\tau = 3/2$ and $\zeta = 4$ for a Brownian force landscape), but *fails* for RF disorder with SR cor-

relations, e.g. $\tau = 0$ and $\zeta = 2$, i.e. for the Gumbel class with $\tau < \tau_{\text{conj}} = 1$.

[59] This hypothesis is proven incorrect in $d = 0$ for the class of short-range correlated forces (random field class)

where one finds on one hand the Sinai-model class in the statics [46] and on the other, the Gumbel extremal statistics class at depinning [56], with vastly different distributions in each class.